

ON THE SPATIAL DISTRIBUTION OF DARK MATTER HALOS

PAOLO CATELAN¹, SABINO MATARRESE² AND CRISTIANO PORCIANI^{3,4}

¹ Theoretical Astrophysics Center, Juliane Maries Vej 30, 2100 Copenhagen Ø, Denmark

² Dipartimento di Fisica ‘G. Galilei’, Università di Padova, via Marzolo 8, 35131 Padova, Italy

³ Scuola Internazionale Superiore di Studi Avanzati, via Beirut 4, 34014 Trieste, Italy

⁴ Space Telescope Science Institute, 3700 San Martin Drive, Baltimore, MD 21218, USA

Ap.J.Letters, in press

ABSTRACT

We study the spatial distribution of dark matter halos in the Universe in terms of their number density contrast, related to the underlying dark matter fluctuation via a non-local and non-linear bias random field. The description of the matter dynamics is simplified by adopting the ‘truncated’ Zel’dovich approximation to obtain both analytical results and simulated maps. The halo number density field in our maps and its probability distribution reproduce with excellent accuracy those of halos in a high-resolution N -body simulation with the same initial conditions. Our non-linear and non-local bias prescription matches the N -body halo distribution better than any Eulerian linear and local bias.

Subject headings: galaxies: statistics – large-scale structure of Universe

1. INTRODUCTION

The simplest description for biasing assumes that the fluctuations in the number density of luminous objects, δ_{lum} , and in the mass, δ_{mass} , are proportional, $\delta_{\text{lum}} = b \delta_{\text{mass}}$, where b is the so called linear *bias factor*. Recently, Catelan et al. (1998, CLMP), following the seminal papers by Cole & Kaiser (1988) and Mo & White (1996, MW), showed how the relation between dark halos, recipient of the luminous matter, and the underlying mass is to be cast in terms of a bias random *field* \mathbf{b} , which depends in a non-local way on the mass density field. Halo biasing is a process which evolves in time, depends on the scales and the collapse times of the selected objects, but is additionally determined by the gravitational conditions of the environment. Most important, unlike previous models, CLMP treated halo biasing as a non-local process.

In this Letter, we apply the CLMP bias model to analyze the spatial halo distribution at several scales. Mass particles move according to the Zel’dovich (1970) approximation. We generally find excellent agreement between our theoretical predictions and the distribution of halos extracted from an N -body simulation with the same initial conditions. In §2 we present our bias model, in §3 we test it against simulations; §4 contains our conclusions.

2. THE DISTRIBUTION OF HALO FLUCTUATIONS

2.1. The model

Let us consider a population of halos, selected in Lagrangian space through their mass M and formation redshift z_f . At any comoving position \mathbf{x} and observation redshift $z \leq z_f$, one can generate Eulerian maps of the halo number density fluctuation $\delta_h(\mathbf{x}, z|M, z_f)$, given the mass density contrast $\delta(\mathbf{x}, z)$ with Lagrangian resolution R_o and the corresponding Lagrangian halo density fluctuation field, $\delta_h^L(\mathbf{q}|M, z_f)$, through the relation

$$\delta_h(\mathbf{x}, z|M, z_f) = [1 + \delta_h^L(\mathbf{q}|M, z_f)] [1 + \delta(\mathbf{x}, z)] - 1, \quad (1)$$

valid in the single-stream regime (CLMP). The non-locality comes from the fact that the halo number density in \mathbf{x} is determined by its initial value at the Lagrangian comoving position \mathbf{q} . Using a local version of the Press & Schechter (1974, PS) approach, we obtain

$$\begin{aligned} \delta_h^L(\mathbf{q}|M, z_f) &= \sqrt{2\pi} [t_f - \epsilon_o(\mathbf{q})] \Theta[t_f - \epsilon_o(\mathbf{q})] \\ &\times \left\{ \sqrt{\frac{\pi}{2}} \frac{t_f \Sigma}{\sigma_M} \left[1 + \text{erf} \left(\frac{t_f \Sigma}{\sqrt{2} \sigma_o \sigma_M} \right) \right] + \sigma_o \exp \left(-\frac{t_f^2 \Sigma^2}{2 \sigma_o^2 \sigma_M^2} \right) \right\}^{-1} \\ &\times \frac{\sigma_M^2}{\Sigma^2} \exp \left[-\frac{\epsilon_o(\mathbf{q})^2 - 2\epsilon_o(\mathbf{q}) t_f + t_f^2 \sigma_o^2 / \sigma_M^2}{2 \Sigma^2} \right] - 1. \quad (2) \end{aligned}$$

This result is obtained as follows: adopting the peak-background split, in the patch of fluid at \mathbf{q} with Lagrangian size R_o , one writes the mean number-density of halos in terms of the PS formula, with a local collapse threshold $t_f - \epsilon_o$ modulated by the background field ϵ_o , and finally removes the overall mean halo number density [eq.(3) below]. Here $t_f \equiv \delta_c / D(z_f)$, with δ_c the critical threshold for collapse of a spherical perturbation and $D(z)$ the linear growth factor of density fluctuations normalized to unity at $z = 0$ [in the Einstein-de Sitter universe, $\delta_c \simeq 1.686$ and $D(z) = (1+z)^{-1}$]; ϵ_o is the linear mass fluctuation extrapolated to $z = 0$ and smoothed on R_o , with σ_o^2 its variance. Finally, $\sigma_M^2 = (2\pi^2)^{-1} \int_0^\infty dk k^2 P(k) W(kR)^2$, with $W(kR)$ the filter function and $P(k)$ the primordial power spectrum, is the variance on scale M of the linear density field ϵ_M and $\Sigma^2 \equiv \sigma_M^2 - \sigma_o^2$. Eq.(2) actually generalizes eq.(42) of CLMP in that collapse on the background scale R_o is accounted for by the step function $\Theta[t_f - \epsilon_o]$: halos of mass $M \propto R^3$ cannot be present in a collapsed region of Lagrangian size $R_o > R$. As stressed by CLMP (see also Porciani et al. 1998), this approach defines catalogs of halos unaffected by the cloud-in-cloud problem (e.g. Bond et al. 1991) up to the scale R_o . By expanding eq.(2) to first order in ϵ_o one obtains, for $\sigma_o \ll \sigma_M$, $\delta_h^L(\mathbf{q}|M, z_f) \simeq b_1^L(M, z_f) \epsilon_o(\mathbf{q})$, where

$b_1^L(M, z_f) \equiv [t_f/\sigma_M^2 - 1/t_f]$ is the linear Lagrangian bias factor (MW). Note that in our approach the background scale R_o appears as a fitting parameter which can be used to optimize the performance of the model. As we will see in §3.2, the optimal value of σ_o generally depends on the chosen Eulerian resolution scale and on the masses of the considered halo population.

When comparing with halos in numerical simulations, we will consider finite mass intervals, so we will have to replace δ_h^L in eq.(2) with its weighted average, where the weight is given by the comoving conditional mass-function

$$n_h(M, z_f) = \frac{\rho_b \exp(-t_f^2/2\sigma_M^2)}{2\pi M \sigma_M^2 \Sigma} \left| \frac{d\sigma_M^2}{dM} \right| \times \left\{ \sqrt{\frac{\pi}{2}} \frac{t_f \Sigma}{\sigma_M} \left[1 + \operatorname{erf}\left(\frac{t_f \Sigma}{\sqrt{2}\sigma_o \sigma_M}\right) \right] + \sigma_o \exp\left(-\frac{t_f^2 \Sigma^2}{2\sigma_o^2 \sigma_M^2}\right) \right\}, \quad (3)$$

with ρ_b the mean density. In addition, as discussed by CLMP, eq.(1) can be generalized to multiple streaming as a Chapman-Kolmogorov-type relation

$$\delta_h(\mathbf{x}, z|M, z_f) = \int d\mathbf{q} [1 + \delta_h^L(\mathbf{q}|M, z_f)] \delta_D[\mathbf{x} - \mathbf{x}(\mathbf{q}, z)] - 1, \quad (4)$$

with δ_D the Dirac function: each fluid element of Lagrangian size R_o carries a ‘halo density charge’ $n_h(M, z_f) [1 + \delta_h^L(\mathbf{q}|M, z_f)]$ along its trajectory.

At every point $\mathbf{x} = \mathbf{q} + \mathbf{S}$, with \mathbf{S} the displacement of the \mathbf{q} -th Lagrangian element smoothed on R_o , we assign a halo density δ_h on the selected mass scale M according to eqs.(2) and (4). We extensively use this formulation of our bias scheme in §3 where we test the model locally against a high-resolution N -body simulation.

2.2. The distribution of halos

In this section we compute the probability distribution $p(\delta_h)$ deriving from our bias model. We consider a mildly non-linear density field in the laminar regime, though for comparisons with simulations we will also adopt the multi-stream generalization in eq.(4).

Eq.(1) can be recast, using mass conservation, in terms of the Jacobian determinant $J \equiv \|\partial\mathbf{x}/\partial\mathbf{q}\|$ of the mapping from Lagrangian to Eulerian space, $\mathbf{q} \rightarrow \mathbf{x}(\mathbf{q}, z) = \mathbf{q} + \mathbf{S}(\mathbf{q}, z)$, namely $1 + \delta[\mathbf{x}, z] = J(\mathbf{q}, z)^{-1}$. In the Zel’dovich approximation, $\mathbf{S}(\mathbf{q}, z) = -D(z)\nabla_{\mathbf{q}}\varphi_o(\mathbf{q})$, where φ_o is the linear peculiar gravitational potential, such that $\nabla_{\mathbf{q}}^2\varphi_o(\mathbf{q}) = \epsilon_o(\mathbf{q})$. The probability distribution of the eigenvalues $\lambda_\alpha(\mathbf{q})$ ($\alpha = 1, 2, 3$) of the deformation tensor $\partial^2\varphi_o(\mathbf{q})/\partial q_\alpha \partial q_\beta$ (Doroshkevich 1970) can be used to compute the one-point statistical properties of δ_h at any redshift $z \leq z_f$ in Eulerian space. Let us introduce the variables $\mathcal{L}_o \equiv \sqrt{5(\mu_1^2 - 3\mu_2)}$, and $\mathcal{P}_o \equiv (\lambda_1 - 2\lambda_2 + \lambda_3)/(2\sqrt{(\mu_1^2 - 3\mu_2)})$, (Reisenegger & Miralda-Escudé 1995) with $\mu_\alpha(\mathbf{q})$ ($\alpha = 1, 2, 3$) the invariants of the deformation tensor. Unlike the original eigenvalues, these variables are independent,

$$p_L(\epsilon_o, \mathcal{L}_o, \mathcal{P}_o) = \left(\frac{e^{-\epsilon_o^2/2\sigma_o^2}}{\sqrt{2\pi}\sigma_o} \right) \left(\frac{2\mathcal{L}_o^4 e^{-\mathcal{L}_o^2/2\sigma_o^2}}{3\sqrt{2\pi}\sigma_o^5} \right) \left(\frac{3}{2} - 6\mathcal{P}_o^2 \right), \quad (5)$$

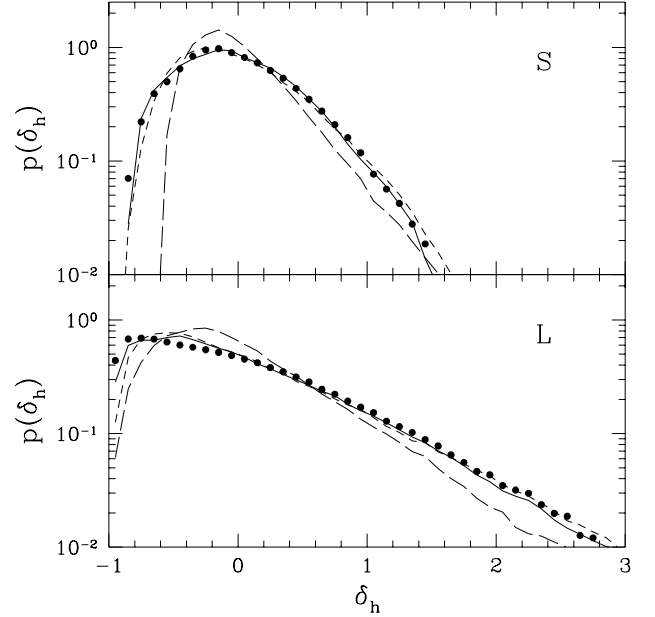


Fig. 1. — The one-point distribution function of δ_h . The short dashed lines refer to the data obtained by performing 10^5 random generations of the variables $\epsilon_o, \mathcal{L}_o$ and \mathcal{P}_o ($k_o = 0.180 h \text{ Mpc}^{-1}$, $\sigma_o^2 = 0.217$); the filled dots show the N -body output. The long dashed lines represent the linear bias prediction while the solid lines are the outcome of the numerical version of our model described in §3.2. Top panels: class S ($k_f = 0.314 h \text{ Mpc}^{-1}$). Bottom panels: class L ($k_f = 0.360 h \text{ Mpc}^{-1}$).

where $0 \leq \mathcal{L}_o \leq \infty$ and $-1/2 \leq \mathcal{P}_o \leq 1/2$. The Jacobian now reads $J = 1 - D\{675\epsilon_o + 45D(\mathcal{L}_o^2 - 5\epsilon_o^2) + D^2[2\sqrt{5}\mathcal{L}_o^3\mathcal{P}_o(3 - 4\mathcal{P}_o^2) - 15\mathcal{L}_o^2\epsilon_o + 25\epsilon_o^3]\}/675$; it enters in eq.(1) through mass conservation.

The probability $p(\delta_h)$ can then be computed by Monte Carlo generating realizations from the distribution in eq.(5). Since we are interested in the Eulerian probability and eq.(5) gives a Lagrangian distribution, we compute $p(\delta_h) = \int d\delta p_L(\delta_h, \delta)/(1 + \delta)$, where $p_L(\delta_h, \delta)$ is the joint Lagrangian probability for the Eulerian halo and mass overdensity fields [cf. eq.(14) in Kofman et al. 1994]. In practice, $p(\delta_h)$ is obtained by: *i*) generating realizations for $\epsilon_o, \mathcal{L}_o, \mathcal{P}_o$; *ii*) computing J , and δ_h through eq.(1) or eq.(4); *iii*) weighting the contribution to the probability of δ_h by the factor J .

3. TESTING THE MODEL

3.1. Comparing the probability distribution function

We test our predictions for $p(\delta_h)$ against a high-resolution N -body simulation from the data bank of cosmological simulations provided by the Hydra Consortium and produced using the Hydra N -body code (Couchman, Thomas & Pierce 1995). The simulation (RUN 501) evolves 128^3 particles on a 128^3 cubic mesh with periodic boundaries. The box size is $100 h^{-1} \text{ Mpc}$ and the particle mass $1.32 \times 10^{11} h^{-1} \text{ M}_\odot$. The initial conditions are Gaussian with a Cold Dark Matter spectrum with shape parameter $\Gamma = 0.25$, density parameter $\Omega = 1$ and zero cosmological constant. The simulation output corresponds to $\sigma_8 = 0.64$, where σ_8 is the rms linear mass fluctuation in spheres of $8 h^{-1} \text{ Mpc}$. At this epoch, the characteristic virializing halo mass, M_* , defined by $\sigma_{M_*} = \delta_c$,

is $0.66 \times 10^{13} h^{-1} M_\odot$, i.e. 50.13 particles. To compare our predictions to the N -body outcome we need a halo catalog from the simulation. We adopt the spherical overdensity (SO) halo-finder (Lacey & Cole 1994) to identify spherical regions with mean overdensity $\kappa = 178$, leading to 5025 halos with more than 20 particles. We then consider two classes of objects: class S contains halos with $0.5 \lesssim M/M_* \lesssim 0.7$; class L has $3 \lesssim M/M_* \lesssim 6$ (see Table 1). In Figure 1 we plot $p(\delta_h)$ obtained with our bias scheme against the N -body outcomes. The model prediction for $z = z_f = 0$ is computed as in §2. σ_o has been tuned to optimize the agreement with the numerical outputs. The simulation probability distribution has been extracted after smoothing the halo distribution by a Gaussian filter $W = \exp(-k^2/2k_f^2)$ with resolution k_f . The prediction of a linear Eulerian bias model is also plotted in Figure 1: the mass distribution in the simulation has been smoothed with the same filter used for the halo overdensity and the resulting δ is multiplied by the Eulerian bias factor $b_{MW} = 1 + [\delta_c/\sigma_M^2 - 1/\delta_c]$ (MW), reported in Table 1. Our model accurately reproduces the tail of the distribution for positive δ_h , while for $\delta_h < 0$ it favours moderate underdensities ($\delta_h \sim -0.5$) with respect to the N -body simulation. The linear bias prescription instead produces much a less skewed distribution with a higher peak and severely underestimates the probability of very underdense regions. Our model can be further improved by adopting the multi-stream version introduced in §3.2, whose predictions, also plotted in Figure 1, are in excellent agreement with the N -body outputs.

3.2. Cross-correlations

We also performed a much more severe point-by-point test, implementing a fully numerical version of our bias scheme as follows. We consider a computational box as large as the N -body one, but sampled with lower resolution: 64^3 particles on a 64^3 grid (using 128^3 particles on a 128^3 mesh gave identical results). Each particle is moved to its final position according to the ‘truncated’ Zel’dovich approximation (Coles et al. 1993), that is, prior computing the displacement, we remove initial power in high frequency modes by a Gaussian filter with resolution k_o ; we require the amplitudes and phases of the linear density field to be identical to the simulation ones (at least for the Fourier modes present in both grids). Each particle is then associated to the linear field $\epsilon_o(\mathbf{q}) = -\nabla_{\mathbf{q}} \cdot \mathbf{S}(\mathbf{q})$. In such a way, every particle is endowed with its own halo-density charge $n_h [1 + \delta_h^L(\mathbf{q})]$, computed as described in §2.1. Note that, while for σ_o^2 we used Gaussian smoothing, σ_M is calculated with top-hat filtering. The halo-density charge is carried by the particles and eventually assigned to the 64^3 grid through the Triangular Shaped Cloud scheme. The corresponding halo overdensity field in the multi-stream regime δ_h^{mod} is then computed and smoothed with a Gaus-

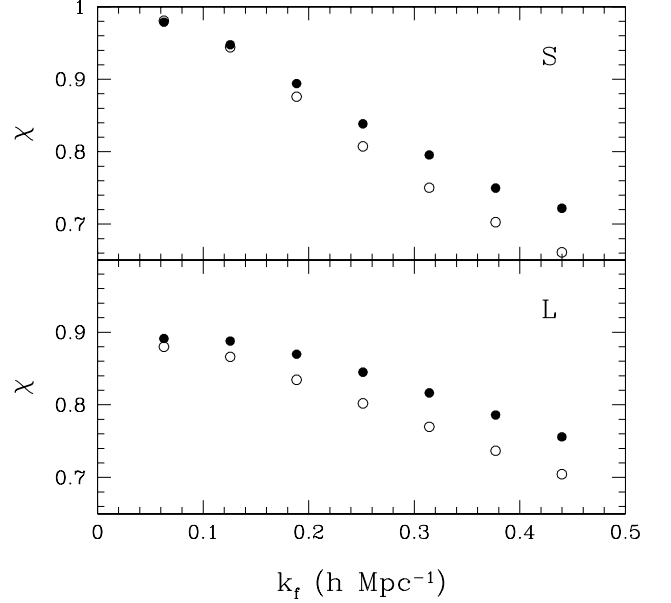


Fig. 2. — Cross correlation coefficients vs. filtering scale. Filled and empty dots represent, respectively, our model and any Eulerian linear bias scheme.

sian filter with $k_f \leq k_o$. The result has to be compared with the halo field δ_h^{sim} extracted from the N -body simulation, smoothed on the same scale. To quantify the agreement between the two, we compute their cross-correlation coefficient $\chi \equiv \langle \delta_h^{\text{mod}} \delta_h^{\text{sim}} \rangle / (\sigma_h^{\text{mod}} \sigma_h^{\text{sim}})$ where $\sigma_h^i \equiv \langle \delta_h^{i2} \rangle^{1/2}$, and the average is performed over the grid points. A value $|\chi| = 1$ means that the two fields are proportional, while $\chi = 0$ for uncorrelated fields. We tune the truncation k_o to optimize our bias scheme. Since χ turns out to depend very weakly on k_o (in a wide range around its optimal value), we can choose it so that $\sigma_h^{\text{mod}} = \sigma_h^{\text{sim}}$ while keeping the maximum allowed value of χ . For each resolution this is obtained with $\sigma_o^2 = 1.65 \sigma_f^2 + C$, with $C = 1.45$ for class S and $C = 0.54$ for class L . Note that in the MW model the value of $\sigma_h^{\text{mod}}/\sigma_h^{\text{sim}}$ is not adjustable and generally differs from 1. For the resolutions considered in Figure 3, $\sigma_h^{\text{mod}}/\sigma_h^{\text{sim}}$ is 0.81 for class S and 0.90 for class L . Moreover, considering smaller smoothing lengths, this ratio can differ from 1 even by 30%. This implies the MW method is unable to accurately predict the average properties of the bias distribution. Figure 2 reports χ values for the optimized model vs. the resolution k_f .

To evaluate the performance of *any* Eulerian linear bias model, we also show the cross-correlation coefficient when the smoothed mass density field from the simulation is used instead of the output mass of our model. This test does not depend on the value of the linear bias. For each smoothing length our model reproduces the halo density field of the simulation much more accurately than the linear biasing scheme. The performance of the two models is similar only for very large smoothing lengths.

In Figure 3 we show the scatter obtained by plotting δ_h^{mod} vs. δ_h^{sim} for our model and for the linear bias scheme. In this case we adopt the MW bias factor in Table 1. Even though on average our bias scheme gives better predictions (especially for class S and for underdense regions), some scatter in the relation δ_h^{mod} vs. δ_h^{sim} persists. To test whe-

TABLE 1
HALO PARAMETERS

Class	N_{min}	N_{max}	#halos	b_{MW}
S	25	35	1021	0.90
L	150	300	466	1.41

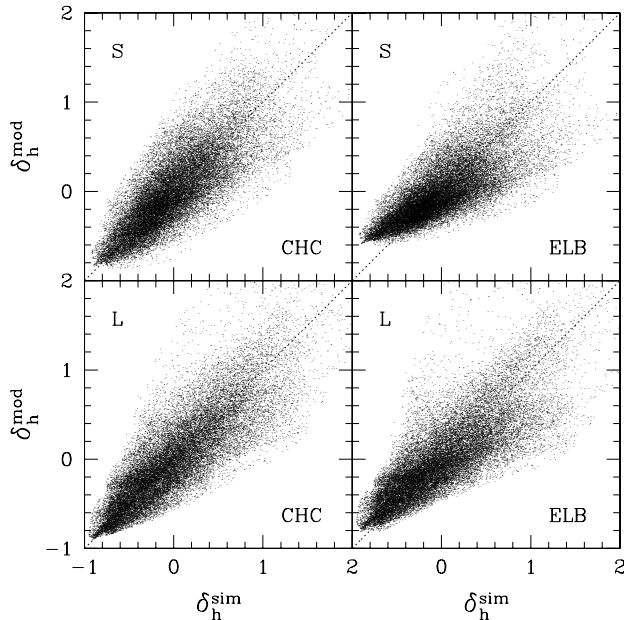


Fig. 3. — Model predictions for δ_h vs. N -body outcome. Left panels: our bias scheme (Conserved Halo-Density Charge, CHC). Right panels: Eulerian Linear Bias model (ELB) in the MW version. Top panels: class S (with $k_f = 0.260 h \text{ Mpc}^{-1}$). Bottom panels: class L (with $k_f = 0.301 h \text{ Mpc}^{-1}$). A 1-in-8 random selection is shown.

ther this is due to our simplified dynamics, we generate new halo maps taking the particle displacements directly from the N -body simulation. The results are in excellent agreement with those obtained with the Zel'dovich approximation, indicating that the local PS approach, being unable to accurately model the Lagrangian halo counting (Fig. 8 in White 1996), is actually responsible for the scatter. We will address this point in a future work.

4. DISCUSSION AND CONCLUSIONS

We devised a simple and fast semi-analytical technique which allows to study the spatial distribution of dark matter halos in terms of their local number density contrast. Our method, which is based on a Lagrangian halo identi-

cation algorithm plus the Zel'dovich approximation for the matter dynamics, was successfully tested against the distribution of halos extracted from a high resolution N -body simulation. Possible improvements should go in the direction of refining the halo selection criterion in Lagrangian space, e.g. using the ellipsoidal collapse model or the peak theory as in (Bond & Myers 1996; see also Monaco 1998).

As stressed by CLMP, our model can be applied to study the evolution of galaxy biasing, once the relation between the galaxies and the hosting dark matter halos is specified (e.g. Matarrese et al. 1997). In particular, defining the bias field such that $\delta_h \equiv b \delta$, from eq.(7) one obtains $b[\mathbf{x}(\mathbf{q}, z), z] = 1 + \delta_h^L(\mathbf{q}|z_f)/[1 - J(\mathbf{q}, z)]$. Tegmark & Peebles (1998) have recently stressed the importance of the asymptotic trend of the bias factor. We can analyze this issue in the present context by considering a galaxy population conserved in number after an initial merging phase (i.e. for varying z at fixed z_f). In the Einstein-de Sitter case we recover the ‘debiasing’ predicted by linear theory: $b \rightarrow 1$ as $z \rightarrow -1$. Differently, if $\Omega < 1$, b tends to a space-dependent value which generally differs from 1; linear theory would predict $b \rightarrow 1 + (b_0 - 1)/D_{-1}(\Omega_0)$, as $z \rightarrow -1$, with $b_0 \equiv b(z=0)$ and $D_{-1} \equiv D(z=-1)$.

Our method can be used to analyze the coarse-grained statistical properties of galaxies and clusters at various redshifts, e.g. applying semi-analytical techniques to relate the dark matter halo distribution to that of luminous objects like galaxies (e.g. Kauffmann, Nusser & Steinmetz 1997). It can be further implemented to generate very large mock maps of these objects in our past light-cone, a problem made of compelling relevance by the ongoing wide-field redshift galaxy surveys like the 2 Degree Field Survey (2dF) and the Sloan Digital Sky Survey (SDSS). Maps of the X -ray cluster distribution may also be produced by the present method.

We thank S. Cole and C. Lacey for providing the SO halo finder and the Hydra Consortium for N -body simulations (<http://coho.astro.uwo.ca/pub/data.html>). PC has been supported by the Danish NRF at TAC; SM and CP by the Italian MURST. CP thanks support from NASA ATP-NAG5-4236 grant.

REFERENCES

- Bond J.R., Cole S., Efstathiou G., Kaiser N., 1991, *ApJ*, 379, 440
- Bond J.R., Myers S.T., 1996, *ApJS*, 103, 1
- Catelan P., Lucchin F., Matarrese S., Porciani C., 1998, *MNRAS*, 297, 692 (CLMP)
- Cole S., Kaiser N., 1989, *MNRAS*, 237, 1127
- Coles P., Melott A.L., Shandarin S.F., 1993, *MNRAS*, 260, 765
- Couchman H.M.P., Thomas P.A., Pearce F.R., 1995, *ApJ*, 452, 797
- Doroshkevich A.G., 1970, *Astrophysics*, 6, 320
- Kauffmann G., Nusser A., Steinmetz M., 1997, *MNRAS*, 286, 795
- Kofman L., Bertschinger E., Gelb J.M., Nusser A., Dekel A., 1994, *ApJ*, 420, 44
- Lacey C., Cole S., 1994, *MNRAS*, 271, 676
- Matarrese S., Coles P., Lucchin F., Moscardini L., 1997, *MNRAS*, 286, 115
- Mo H.J., White S.D.M., 1996, *MNRAS*, 282, 347 (MW)
- Monaco P., 1998, *Fund Cosm Phys*, 19, 157
- Porciani C., Matarrese S., Lucchin F., Catelan P., 1998, *MNRAS*, in press (astro-ph/9801290)
- Press W.H., Schechter P., 1974, *ApJ*, 187, 425
- Reisenegger A., Miralda-Escudé J., 1995, *ApJ*, 449, 476
- Tegmark M., Peebles P.J.E., 1998, *ApJL*, in press
- White S.D.M., 1996, in *Cosmology and Large Scale Structure*, eds. Schaeffer R., Silk J., Spiro M., Zinn-Justin J., Elsevier, p.349
- Zel'dovich Ya.B., 1970, *A&A*, 5, 84